Monthly Notices
of the
ROYAL ASTRONOMICAL SOCIETY

MNRAS **478,** 825–834 (2018)
Advance Access publication 2018 April 27

doi:10.1093/mnras/sty1070

Optical turbulence profiling with Stereo-SCIDAR for VLT and ELT

J. Osborn,[1]★ R. W. Wilson,[1] M. Sarazin,[2] T. Butterley,[1] A. Chacón,[2] F. Derie,[2] O. J. D. Farley,[1] X. Haubois,[2] D. Laidlaw,[1] M. LeLouarn,[2] E. Masciadri,[3] J. Milli,[2] J. Navarrete[2] and M. J. Townson[1]

[1]*Centre for Advanced Instrumentation, University of Durham, Durham, UK*
[2]*European Southern Observatory, Karl-Schwarzshild-Str 2, D-85748 Garching bei Muenchen, Germany*
[3]*INAF Osservatorio Astrofisico di Arcetri, Largo Enrico Fermi 5, I-50125 Florence, Italy*

Accepted 2018 April 17. Received 2018 April 17; in original form 2018 February 19

ABSTRACT

Knowledge of the Earth's atmospheric optical turbulence is critical for astronomical instrumentation. Not only does it enable performance verification and optimization of the existing systems, but it is required for the design of future instruments. As a minimum this includes integrated astro-atmospheric parameters such as seeing, coherence time, and isoplanatic angle, but for more sophisticated systems such as wide-field adaptive optics enabled instrumentation the vertical structure of the turbulence is also required. Stereo-SCIDAR (Scintillation Detection and Ranging) is a technique specifically designed to characterize the Earth's atmospheric turbulence with high-altitude resolution and high sensitivity. Together with ESO (European Southern Observatory), Durham University has commissioned a Stereo-SCIDAR instrument at Cerro Paranal, Chile, the site of the Very Large Telescope (VLT), and only 20 km from the site of the future Extremely Large Telescope (ELT). Here we provide results from the first 18 months of operation at ESO Paranal including instrument comparisons and atmospheric statistics. Based on a sample of 83 nights spread over 22 months covering all seasons, we find the median seeing to be 0.64″ with 50 per cent of the turbulence confined to an altitude below 2 km and 40 per cent below 600 m. The median coherence time and isoplanatic angle are found as 4.18 ms and 1.75″, respectively. A substantial campaign of inter-instrument comparison was also undertaken to assure the validity of the data. The Stereo-SCIDAR profiles (optical turbulence strength and velocity as a function of altitude) have been compared with the Surface-Layer Slope Detection And Ranging, Multi-Aperture Scintillation Sensor-Differential Image Motion Monitor, and the European Centre for Medium Range Weather Forecasts model. The correlation coefficients are between 0.61 (isoplanatic angle) and 0.84 (seeing).

Key words: atmospheric effects – instrumentation: adaptive optics – site testing – telescopes.

1 INTRODUCTION

Turbulence within the Earth's atmosphere imposes a limitation upon astronomical observations. Wavefront distortions blur the image and can be compensated with Adaptive Optics (AO) systems. The future of this correction technique requires comprehensive knowledge of the dynamics of the Earth's atmosphere. This is critical for future sophisticated AO systems on the existing very large and the future extremely large telescopes (ELTs). These telescopes will be sensitive to variations in turbulence altitude of the order of 100 to 500 m (see Neichel, Fusco & Conan 2008; Basden, Myers & Butterley 2010; Vidal, Gendron & Rousset 2010; Gendron et al. 2014).

The next generation of 40 m class ELTs that are currently under construction will enable new discoveries in all areas of astronomy and push forward the boundaries of human knowledge. They will look further back in space and time to explore the early universe and shed light on currently unanswered questions such as the physical basis of dark energy and dark matter, as well as their evolution in the time-scales from early Universe to present time. They will discover and characterize extra-solar planets and potentially find distant habitable worlds. More details of ELT science cases can be found in European Southern Observatory (2009); Skidmore & Committee (2015). To fulfil these ambitious objectives these giant telescopes will be equipped with highly sophisticated AO in order to counteract the detrimental effects of the Earth's atmosphere.

SCIDAR (Scintillation Detection and Ranging) (Vernin & Roddier 1973) is a technique often used for profiling the Earth's

★ E-mail: james.osborn@durham.ac.uk

atmospheric turbulence. Stereo-SCIDAR is an extension of the SCIDAR technique. Stereo-SCIDAR is a sensitive, high-altitude resolution turbulence monitor capable of returning the vertical profile of Earth's optical turbulence strength and velocity in real-time. The Stereo-SCIDAR instrument has been described previously (Shepherd et al. 2014). It has been routinely and reliably used at the Observatorio del Roque de Los Muchachos, La Palma, Spain, (Osborn et al. 2015a), and more recently at ESO Paranal. There is also a version under development for Mount Stromlo, Australia (Korkiakoski et al. 2016).

The wind velocity profiles from Stereo-SCIDAR have been validated with both balloon borne radiosonde and General Circulation numerical weather forecast models from the Global Forecast System (Osborn et al. 2017). This multi-way comparison shows that the numerical models are capable of forecasting wind profiles for astronomical instrumentation optimization on average but if high-temporal resolution variations are of interest then the optical monitor is still required.

Recent applications of Stereo-SCIDAR include supporting the AO testbed, Canary (Morris et al. 2014), where it was used to validate the tomographic reconstructor as well as to validate the Linear Quadratic Gaussian smart AO controller (Sivo 2014).

Here we specifically discuss the Stereo-SCIDAR commissioned by ESO to operate at Cerro Paranal, Chile, the site of the Very Large Telescope (VLT). The VLT comprises of four 8 m unit telescopes (UT) and four 1.8 m auxiliary telescopes (AT), and only 20 km from the site of the future ELT. Stereo-SCIDAR was commissioned at ESO Paranal in April 2016 and has been in regular operation since this date. The Stereo-SCIDAR profiles are of particular and current interest at Paranal due to the development of wide-field view AO system on the VLT and the planned AO systems on the ELT. The optical turbulence profiles will enable performance estimation as well as performance validation of these complicated tomographic AO systems.

We compare the results from Stereo-SCIDAR with the existing Paranal suite of dedicated site monitors, including the Surface-Layer Slope Detection And Ranging (SLODAR) instrument (Wilson 2002; Osborn et al. 2010; Butterley et al. 2015), and the Multi-Aperture Scintillation Sensor-Differential Image Motion Monitor (MASS-DIMM) (Sarazin & Roddier 1990; Sarazin, Cuevas & Navarrete 2011; Kornilov et al. 2003). We also compare the wind velocity profiles from the Stereo-SCIDAR with those from the European Centre for Medium Range Weather Forecasts (ECMWF) (Osborn et al. 2017). Using the three instruments and the model in this way it is possible to validate the performance of the recently commissioned Stereo-SCIDAR instrument.

After instrumentation cross-validation we present the results, statistics, and temporal variations from the Stereo-SCIDAR instrument with respect to the main applications:

(i) Astronomical instrumentation performance monitoring and validation. This will require sequences of turbulence profiles and corresponding astro-atmospheric parameters, such as seeing, coherence time, and isoplanatic angle.

(ii) Astronomical instrument design. All future instrumentation needs to be designed for the specific atmospheric conditions they are expected to encounter. The Stereo-SCIDAR will provide distributions of astro-atmospheric parameters and the median optical turbulence profile, which is critically important for the future generation of wide-field AO.

(iii) Real-time instrument optimization.

(iv) General site monitoring.

(v) Meso-scale atmospheric turbulence forecasting calibration and validation (Masciadri et al. 2017).

There has been a lot of previous work on characterizing the Earth's turbulent atmosphere above ESO Paranal.

The DIMM has been in regular operation on site since 1990 and therefore provides a large sample to derive integrated turbulence statistics (Sarazin et al. 2008).

Other studies such as the multi-instrument campaign of 2007 (Sarazin & Roddier 1990; Kornilov et al. 2003; Ziad et al. 2004; Maire et al. 2007; Ramió et al. 2008; Tokovinin, Bustos & Berdja 2010; Dali Ali et al. 2010) and the surface layer characterization campaign of 2010 (Sarazin & Roddier 1990; Kornilov et al. 2003; Lombardi et al. 2010; Osborn et al. 2010; Tokovinin et al. 2010), were extremely useful for understanding the atmosphere and the various instruments. However due to the limited nature of the campaigns they do not attempt to present a statistical representation of the site.

Cute-SCIDAR, another SCIDAR instrument was operational at ESO Paranal during November/December 2007 (Ramió et al. 2008; Masciadri et al. 2011). This SCIDAR operated for 20 nights and was used as part of the Paranal 2007 multi-instrument campaign (Dali Ali et al. 2010). The data from this instrument have proved extremely useful to further the understanding of the behaviour of the MASS (Masciadri, Lombardi & Lascaux 2014; Lombardi & Sarazin 2016).

With the exception of the MASS-DIMM these campaigns provide a limited data set with which to compare our data. Here, we present the first 20 months of Stereo-SCIDAR operation which significantly increases the volume of high-altitude resolution and high-sensitivity turbulence profiles at ESO Paranal.

Section 2 describes the instrument, the data analysis pipeline, and the data archive. Section 3 shows the distribution of the turbulence statistics as measured by the first phase of the Stereo-SCIDAR operation at Paranal. The comparisons of the parameters as estimated by Stereo-SCIDAR are compared to other existing instrumentation in Section 4. The conclusions are in Section 5.

2 STEREO-SCIDAR

The Stereo-SCIDAR method has been described in detail several times before (see Shepherd et al. 2014; Osborn et al. 2015a, 2017; Derie et al. 2016).Briefly, the Stereo-SCIDAR uses the triangulation technique by cross-correlating the spatial intensity pattern (scintillation) from two stars. The offset of the correlation peak indicates the altitude of the turbulence and the magnitude of the correlation peak indicates the strength of the turbulence. The wind velocity can be estimated by measuring the velocity of the correlation peak when temporal delays are added between the images from the two stars. The advantage of Stereo-SCIDAR over previous generalized SCIDAR instruments comes from using two detectors, one for each target. This increases the sensitivity as the scintillation patterns are optically separated, rather than overlapping on a single detector that reduces the contrast. Using two detectors also enables a greater magnitude difference in the target stars, increasing the usable target catalogue and hence sky coverage.

2.1 Data analysis pipeline

The data analysis generally follows the routine described in Shepherd et al. (2014) and Osborn et al. (2017), with some significant changes. In Shepherd et al. (2014) we fit a response function to ev-

ery pixel separation. This implied a vertical resolution equal to one pixel offset, i.e. z_{max}/n_{pix}, where n_{pix} is the number of pixels across the pupil image of the telescope and z_{max} is the maximum propagation distance that the Stereo-SCIDAR can sense, given by D/θ, where D is the telescope diameter and θ is the stellar separation. However, in reality the vertical resolution of the Stereo-SCIDAR is altitude dependent, with larger propagation distances (higher turbulent zones) resulting in broader response functions (up to several pixels in size). Using a response function for every pixel separation will lead to the inverse problem being ill-conditioned. Instead, the response functions are separated by a distance of $0.5\sqrt{\lambda z}$, where λ is the wavelength of the light and z is the propagation distance. In this way the response function separation is altitude dependent and reflects the native resolution of the Stereo-SCIDAR instrument (Avila, Vernin & Cuevas 1998), reducing noise due to the ill-conditioned inversion problem. We calculate the response functions for a monochromatic wavelength of 500 nm. A dichroic filter is used to reflect light with wavelengths longer then 600 nm to the acquisition camera and the Andor Luca EMCCD (Electron Multiplying Charge Coupled Device) detectors have a cut-off at 400 nm.

The wind velocities are found by measuring the motion of the cross-covariance peaks in the temporal spatio-cross covariance function. Initially the correlation peaks are found by applying a CLEAN-like algorithm to the spatio-temporal cross-covariance function, similar to that described in Prieur et al. (2004). The velocities are then estimated by finding sets of at least five covariance peaks that appear to move in a straight line with a constant velocity (Osborn et al. 2017). However, some layers can be missed in the wind velocity profile. For weak turbulence it is difficult to identify wind vectors in the Stereo-SCIDAR data and due to this limitation we cannot guarantee to measure all of the turbulence velocity vectors.

The contribution of optical turbulence in the dome is subtracted from all the Stereo-SCIDAR measurements automatically. Using the assumption that the dome turbulence evolves slowly we can monitor the decorrelation of the covariance peak corresponding to local turbulence and extrapolate to estimate the magnitude of the dome turbulence. This is an extension of the method proposed by Avila et al. (1998) and is described in Shepherd et al. (2014).

The data are analysed automatically in real time providing a real-time display that updates with new data approximately every 120 s. Fig. 1 is an example of this real-time display.

2.2 Data archive

Table 1 summarizes the data set used in this study. The total hours are found by adding together the duration of each data set (i.e. it does not include gaps in the data due to change of targets or bad weather). Although the data represents times distributed throughout the year over a period of almost two years, it is still a limited data set. Stereo-SCIDAR will continue to operate while it can be supported by ESO, however, here we show the results for the first phase of the project. The data are available upon request to the author and the archive will continue to grow as more data are collected. The data will be released in batches comprising a data release. The data used for this study are data release '2018A'. The profiles have been linearly interpolated into 250 m altitude bins and normalized such that the integrated turbulence strength is conserved. The profiles are padded with '−1' above the maximum profiling altitude to maintain the same number of bins per profile. The dome seeing has been subtracted. The 'native' resolution (un-interpolated) profiles are also available on request to the author.

3 PARAMETER STATISTICS

Fig. 2 shows the median turbulence strength as a function of altitude above observatory level. The median profile cannot be used as a typical profile. However, it does give an estimate of the expected turbulence strength at each altitude.

Stereo-SCIDAR provides measurements of the strength of the optical turbulence, quantified by the refractive index structure parameter, $C_n^2(h)$, as a function of altitude, h, the turbulence speed, $|V(h)|$, and direction $V_\theta(h)$. Using these functions it is possible to derive a number of other optical parameters:

$$r_0 = \left(0.423\left(\frac{2\pi}{\lambda}\right)^2 \cos(\gamma)^{-1}\int C_n^2(h)\mathrm{d}h\right)^{-3/5}, \quad (1)$$

$$\epsilon = \frac{0.98\lambda}{r_0}, \quad (2)$$

$$\theta_0 = \left(2.914\left(\frac{2\pi}{\lambda}\right)^2 \cos(\gamma)^{-8/3}\int C_n^2(h)h^{5/3}\mathrm{d}h\right)^{-3/5}, \quad (3)$$

$$\tau_0 = \left(2.914\left(\frac{2\pi}{\lambda}\right)^2 \cos(\gamma)^{-8/3}\int \frac{C_n^2(h)}{V(h)^{5/3}}\mathrm{d}h\right)^{-3/5}, \quad (4)$$

$$\sigma_I^2 = 10.7D^{-4/3}t^{-1}\cos(\gamma)^{\alpha(V_\theta(h))}\int \frac{C_n^2(h)h^2}{V(h)}\mathrm{d}h, \quad (5)$$

where r_0 is the Fried parameter (Fried 1966), ϵ is the Full-Width at Half Maximum (FWHM) of the point spread function (PSF) or seeing on a small telescope, θ_0 is the isoplanatic angle (Roddier 1981), τ_0 is the coherence time (Greenwood 1978), and σ_I^2 is the scintillation variance on a telescope of diameter larger than a few tens of centimetres and for long exposures (Dravins et al. 1997; Osborn et al. 2015b). Other required parameters for the above calculations are the zenith angle, γ, the wavelength of the observation, λ, the telescope diameter, D, the observation exposure time, t, and the air mass exponent, α. Note that the value of the airmass exponent, α, will depend on the wind direction and vary between -3 for the case when the wind is transverse to the azimuthal angle of the star, and up to -4 in the case of a longitudinal wind direction. This is a geometric correction. In the case where the wind direction is parallel to the azimuthal angle of the star, the projection of the telescope pupil on to a horizontal layer is stretched by a factor of $1/\cos(\gamma)$, which changes the projected wind speed. Therefore, $\alpha = -3.5 + \cos 2(V_\theta - \theta_{az})/2$, where θ_{az} is the azimuthal angle of the observation. Further discussion of scintillation in astronomical time-resolved photometry for smaller telescopes and short exposures can be found in Osborn et al. (2015b).

Each of these parameters has its own influence for particular applications. r_0 and ϵ are both used to measure the effect on an image caused by a wavefront that has propagated through the complete atmosphere. The isoplanatic angle defines the angular extent over which the atmospheric effects are correlated. It is this parameter that defines the angular size of an AO-corrected field. Multi-Conjugate Adaptive Optics (MCAO) systems can be used to increase the isoplanatic angle and hence increase the corrected field of view. The coherence time defines the update rate that an AO system must function at in order to minimize residual wavefront errors due to the temporal lag between the wavefront measurements and correction by the deformable mirror (DM). All of this information can be used

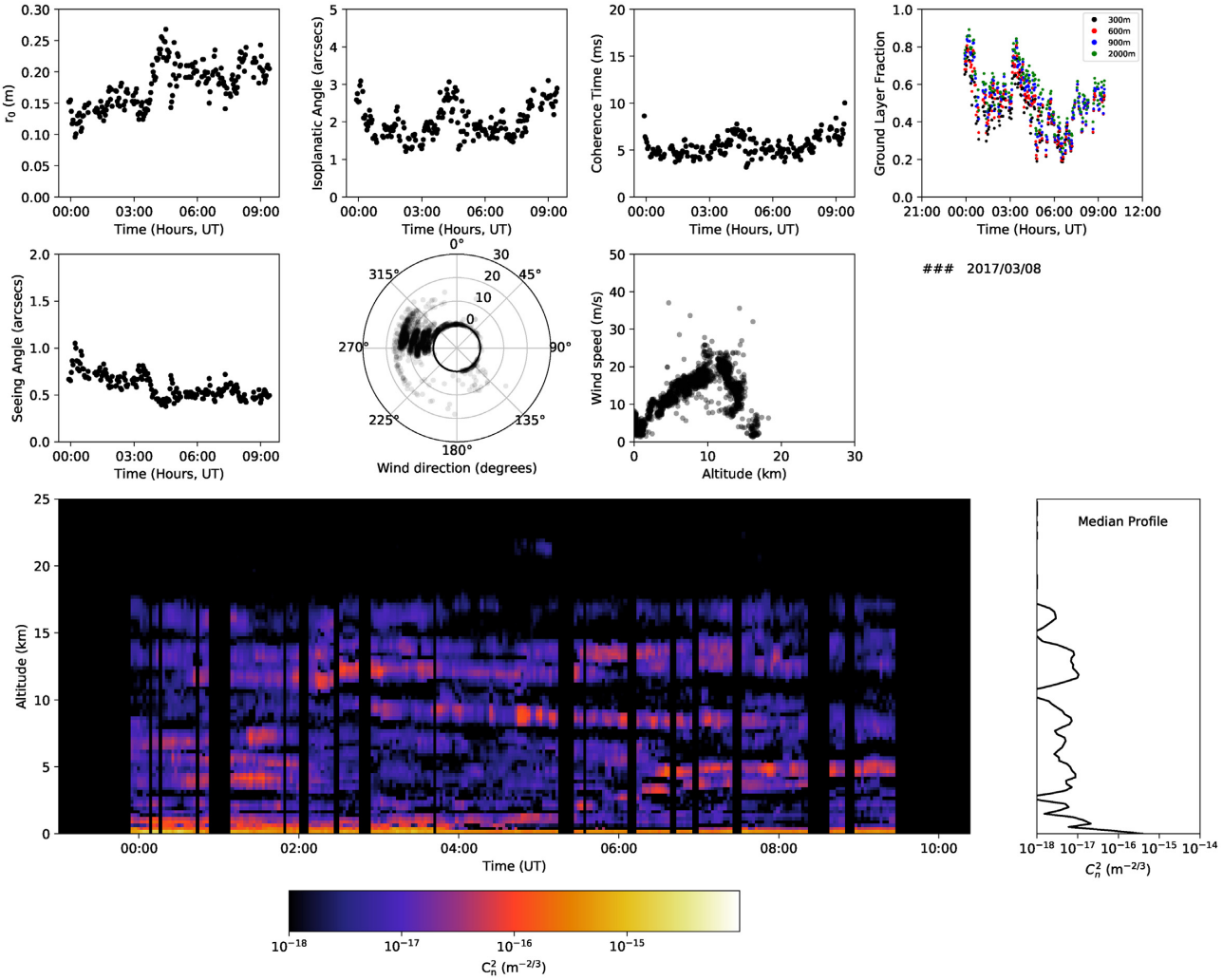

Figure 1. Example Stereo-SCIDAR real-time display for the night beginning 2017 March 8. The radial numbers on the wind direction polar plot denotes the altitude above the observatory in kilometers. The transparency of the data points denotes the time since the data were taken.

Table 1. ESO Paranal, Stereo-SCIDAR data volume: 2018A.

Year	Month	Days	Hours	Number of Profiles
2016	April	26–29	18.43	607
	July	22–26	37.12	1143
	October	30–31	10.65	301
	November	1–2	10.80	302
	December	10–12	11.62	308
2017	March	7–9	16.46	469
	April	12–18	37.34	988
	May	5–9	16.06	419
	June	8–10	19.97	511
	July	3–9	37.60	962
	August	3–8	34.42	930
	November	4–9, 18–20, 29–30	45.63	1076
	December	1–6, 8–18	56.69	1483
2018	January	13–24	44.19	1192
Totals:		83	396.97	10691

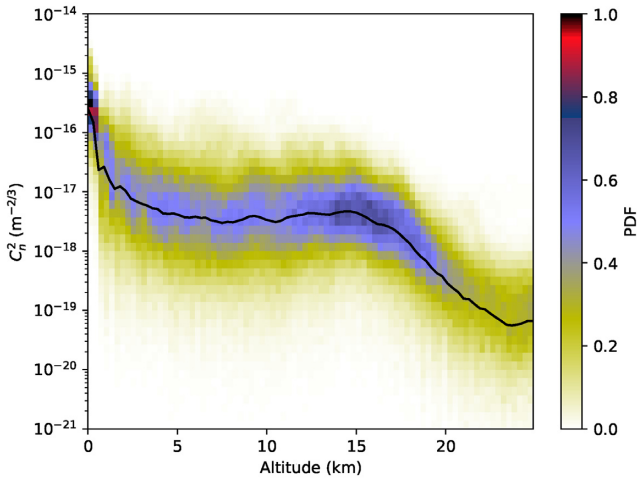

Figure 2. The median optical turbulence strength profile from Stereo-SCIDAR at the Cerro Paranal. The black line shows the median. The colour shows the distribution of the turbulence strength at each altitude.

Table 2. Astro-atmospheric parameter statistics for Paranal for the Stereo-SCIDAR from data release 2018A.

Parameter	Q1	Median	Q3
Seeing	0.52″	0.64″	0.85″
Coherence Time	2.82 ms	4.18 ms	6.65 ms
Isoplanatic Angle	1.34″	1.75″	2.22″
Scintillation Index (1m,1s,$\times 10^{-5}$)	0.39	0.63	1.04
GF ($h < 300$ m)	0.14	0.25	0.38
GF ($h < 600$ m)	0.25	0.40	0.57
GF ($h < 900$ m)	0.29	0.45	0.62
GF ($h < 1200$ m)	0.34	0.49	0.65

in real time for AO support, PSF reconstruction, observatory, and observation scheduling.

The scintillation index is critical for time-resolved photometry. Here, we show the scintillation index for a 1-mtelescope and 1 s exposure, such that it can easily be scaled to other system specifications.

The fraction of the turbulence in the ground layer is also a parameter of significant interest to observatories with interests in wide-field view AO instrumentation, such as Ground-Layer AO. The performance and the uniformity of correction of wide-field AO systems is very dependent on the structure of the atmospheric optical turbulence profile. Here we present the ground layer fraction (GF), defined as the ratio of the turbulence strength up to the given altitude to the integrated turbulence up to the maximum sensing altitude, up to 300, 600, 900, and 1200 m.

In addition to the above, statistical data on the typical profiles and variability of each of the profiles can be used for instrument development and performance analysis (Morris 2014).

In Table 2 we show the first, second, and third quartile of each of the parameters of interest.

It is interesting to compare these values to previous studies. In Sarazin et al. (2008) the authors show that the seeing at Paranal, as measured by the original DIMM has actually increased over the years from a median of 0.65″ to a median of 1.1″, whereas the seeing from the UT image quality measurements of FORS2, an instrument on the VLT, has remained at 0.65″. The authors of that study suggest that this discrepancy is likely caused by a thin strong ground layer that is becoming more frequent and the effect on the original DIMM was exacerbated by its location close to the 20 m high VLT Survey Telescope. The instruments on the UTs are protected from this low-altitude turbulence by the telescope dome. In this study, we compare with a new DIMM in a new location, further from any buildings and on a higher tower. The new DIMM reports a median seeing of 0.63″ (during Stereo-SCIDAR runs), which is compatible with the Stereo-SCIDAR measurements and indeed with the UT image quality measurements.

The distributions of these parameters are shown in Figs 3 and 4. Fig. 5 shows the distribution of the fraction of the turbulence up to any given altitude. For example, the figure shows that approximately 50 per cent of the turbulence strength is confined to an altitude below 2.0 km, however this value is variable and can actually range between 0.2 and 0.8.

4 INSTRUMENT COMPARISONS

The Stereo-SCIDAR outputs, turbulence strength, and velocity vertical profiles are compared with other instruments on the Paranal site. Comparisons are made for measurements between the Stereo-

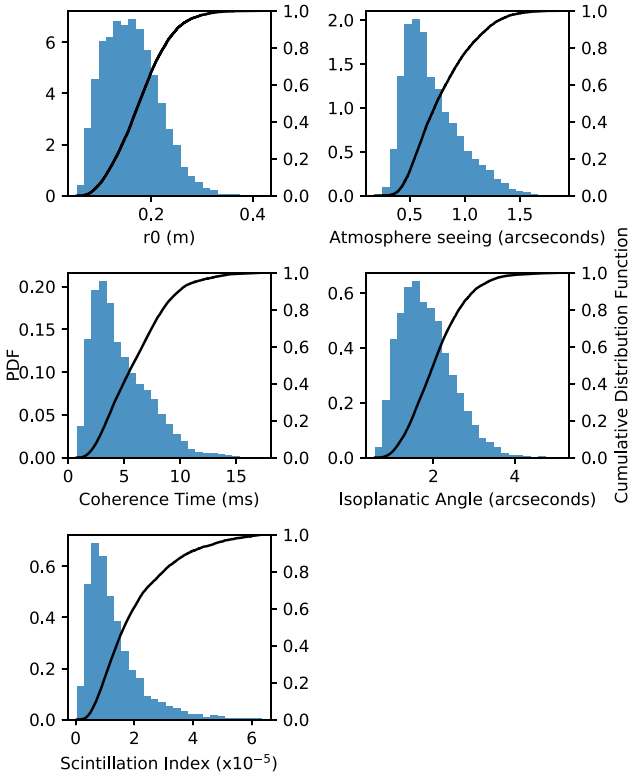

Figure 3. The distribution of r_0, seeing, coherence time, isoplanatic angle, and scintillation noise (scaled to 1 m telescope with 1 s exposure time) with cumulative density function overlaid as the solid line.

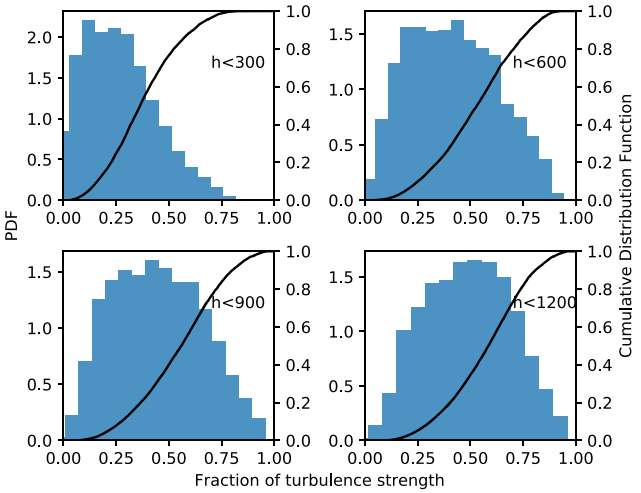

Figure 4. Distributions of the fractions of turbulence below an altitude h. The fractional turbulence distributions, together with the cumulative distribution, is shown for four altitudes, $h < 300$ m, 600 m, 900 m, and 1200 m (top left, top right, bottom left, and bottom right, respectively). The fraction of turbulence can be seen increasing as we integrate up to higher altitudes, as expected. However, the width of the distribution is of particular interest. On some occasions, up to 75 per cent of the turbulence can be found in the first 300 m.

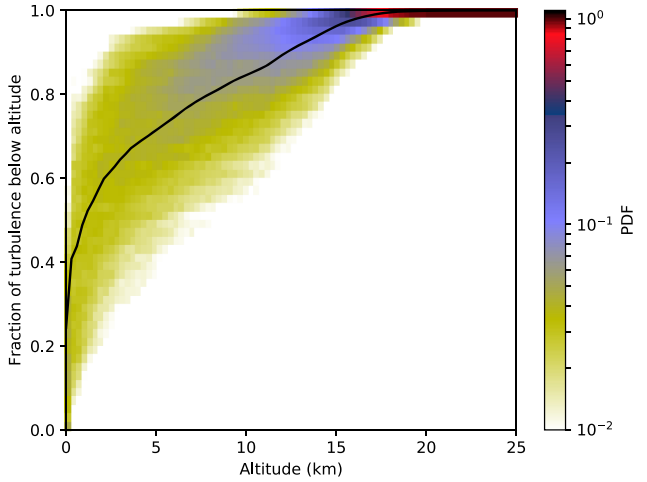

Figure 5. Distribution of integrated turbulence up to an altitude. The colour indicates the distribution of the fraction of turbulence below a given height, such that a wide spread indicates a large range of values. The median is shown by the solid line. For example, approximately 50 per cent of the turbulence strength is confined to an altitude below 2.0 km, however this value can actually range between 0.2 and 0.8 as shown by the colour.

SCIDAR and the alternative instrument/model for measurements taken within 5 min of each other. If more than one measurement was made within the time frame the median value is used in the comparison. The mean value provides a very similar answer to the median (<1 per cent difference in comparison parameters), and so is not reported here. The instruments were spatially separated and were not observing the same targets. The parameters for all instruments are corrected for zenith angle.

Table 3 shows the instruments and their corresponding metrics for the comparisons. We see that generally the correlation between the instrumentation (and the model in the case of the ECMWF) is high. In the following sections we will discuss each comparison in more detail. We also show the values for the Stereo-SCIDAR compared with itself averaged over the 5 min comparison period. This is done to show the spread of the data expected from comparing two measurements in the sampling period.

The map of the Paranal site complete with telescopes and instrumentation is shown in Fig. 6. It can be seen that the Stereo-SCIDAR is located in the centre of the platform, whereas the other site-monitoring instrumentation is located near the edge of the platform. This may have an effect on the magnitude of the measured optical turbulence near the ground.

4.1 MASS-DIMM

The MASS-DIMM is a combination of two instruments: a DIMM to measure the integrated seeing (Sarazin & Roddier 1990) and a MASS channel to perform low-resolution profiling (Tokovinin & Kornilov 2007). The MASS-DIMM also estimates the isoplanatic angle from these low-resolution profiles and the coherence time from the variance of the logarithm of the intensity ratio for different exposure times (Sarazin et al. 2011).

Due to technical issues the MASS-DIMM was unavailable between 2017 February 1 to 2017 May 19. For this reason we only have 68 nights of overlap between the MASS-DIMM and the Stereo-SCIDAR.

Fig. 7 shows the comparison between the Stereo-SCIDAR and the MASS-DIMM for the integrated seeing, free atmosphere seeing, the coherence time, and the isoplanatic angle. In all cases the correlation is high, between 0.61 for the isoplanatic angle and 0.84 for the seeing. The free atmosphere seeing is found by projecting the Stereo-SCIDAR on to the MASS-DIMM weighting functions to take into account the non-uniform response of the MASS-DIMM to turbulence, particularly in the 250 m to 500 m altitude range. The reason for the lower correlation in the isoplanatic angle comparison might be due to the low-altitude resolution profiles from the MASS used in the calculation, as suggested by the relatively large RMSE but low bias. The shape of the seeing comparison curve is interesting as it shows a trend for the Stereo-SCIDAR to measure less turbulence in stronger seeing conditions. This could either be due to a bias in one of the instruments in bad seeing (due to scintillation saturation in the Stereo-SCIDAR for example) or a physical manifestation due to the spatial separation of the instruments. The Stereo-SCIDAR is located in the centre of the observing platform, whereas the MASS-DIMM is located at the edge. Therefore the MASS-DIMM may encounter elevated seeing due to the strong turbulence at the edge of the platform in certain conditions (certain wind directions for example). From Fig. 8 we can see that the high-seeing tail corresponds to periods of high ground layer strength. This supports the argument that the difference is due to location of the instruments (as suggested by Sarazin et al. 2008).

4.2 Surface-Layer SLODAR

The Surface-Layer SLODAR is a fully robotic and automatic turbulence profiler designed to profile the lowest region of the Earth's atmosphere with high vertical resolution (Osborn et al. 2010; Butterley et al. 2015). SLODAR is a crossed-beams technique, such as SCIDAR, that uses a Shack–Hartmann wavefront sensor to observe bright double star targets. As the method is based on direct measurements of the wavefront phase gradient, it is relatively straightforward to calibrate in terms of the absolute optical turbulence profile (Butterley, Wilson & Sarazin 2006). Surface-Layer SLODAR uses wide optical binary stars to probe the lower atmosphere, up to a few hundred metres, with an altitude resolution of a few tens of metres. The exact values depend on the separation of the target stars and airmass.

Fig. 9 shows the comparison of the Stereo-SCIDAR and the Surface-Layer SLODAR integrated seeing from the height of the ESO VLT AT (5 m) upwards. We see a high correlation between the two measurements, however there is a small bias for Surface-layer SLODAR to measure more integrated turbulence than the Stereo-SCIDAR. This is likely to be due to the locations of the instruments. The Stereo-SCIDAR is located on the centre of the observing platform away from the edges of the mountain. However, the Surface-Layer SLODAR, like the MASS-DIMM, is located near to the edge of the platform where local turbulence can be higher.

4.3 ECMWF

General circulation models (GCM) have been used to provide wind velocity profiles for previous astronomical studies (e.g., Hagelin, Masciadri & Lascaux 2010; Osborn et al. 2017). They have also been used as the input for mesoscale turbulence forecast models (for example, for the wind velocity profile Masciadri, Lascaux & Fini 2013 and for the turbulence strength profile Giordano et al. 2013; Masciadri et al. 2017). In this study, we use the ECMWF to

Table 3. Astro-atmospheric parameter comparison for Paranal for the Stereo-SCIDAR with the Surface Layer SLODAR, MASS-DIMM, and the wind velocities from the ECMWF. The comparison is in terms of the Pearson correlation coefficient (C), bias, and root-mean-square error (RMSE). We also show the values for the Stereo-SCIDAR compared with itself averaged over the 5 min comparison period.

Instrument	Parameter	C	Bias	RMSE
SL-SLODAR	Seeing (h > 5 m)	0.73	− 0.04″	0.20″
MASS-DIMM	Seeing	0.84	− 0.11″	0.21″
	Free Atmosphere Seeing (MASS)	0.84	0.02″	0.14″
	Coherence Time	0.73	− 0.11 ms	2.01 ms
	Isoplanatic Angle	0.61	− 0.10″	0.63″
ECMWF	Wind Speed	0.82	0.41 m s^{-1}	6.44 m s^{-1}
	Wind Direction	0.77	1.59 deg	27.09 deg
Stereo-SCIDAR	Seeing	1.00	0.06″	0.24″
	Coherence time	1.00	0.51 ms	2.20 ms
	Isoplanatic angle	1.00	0.12″	0.69″

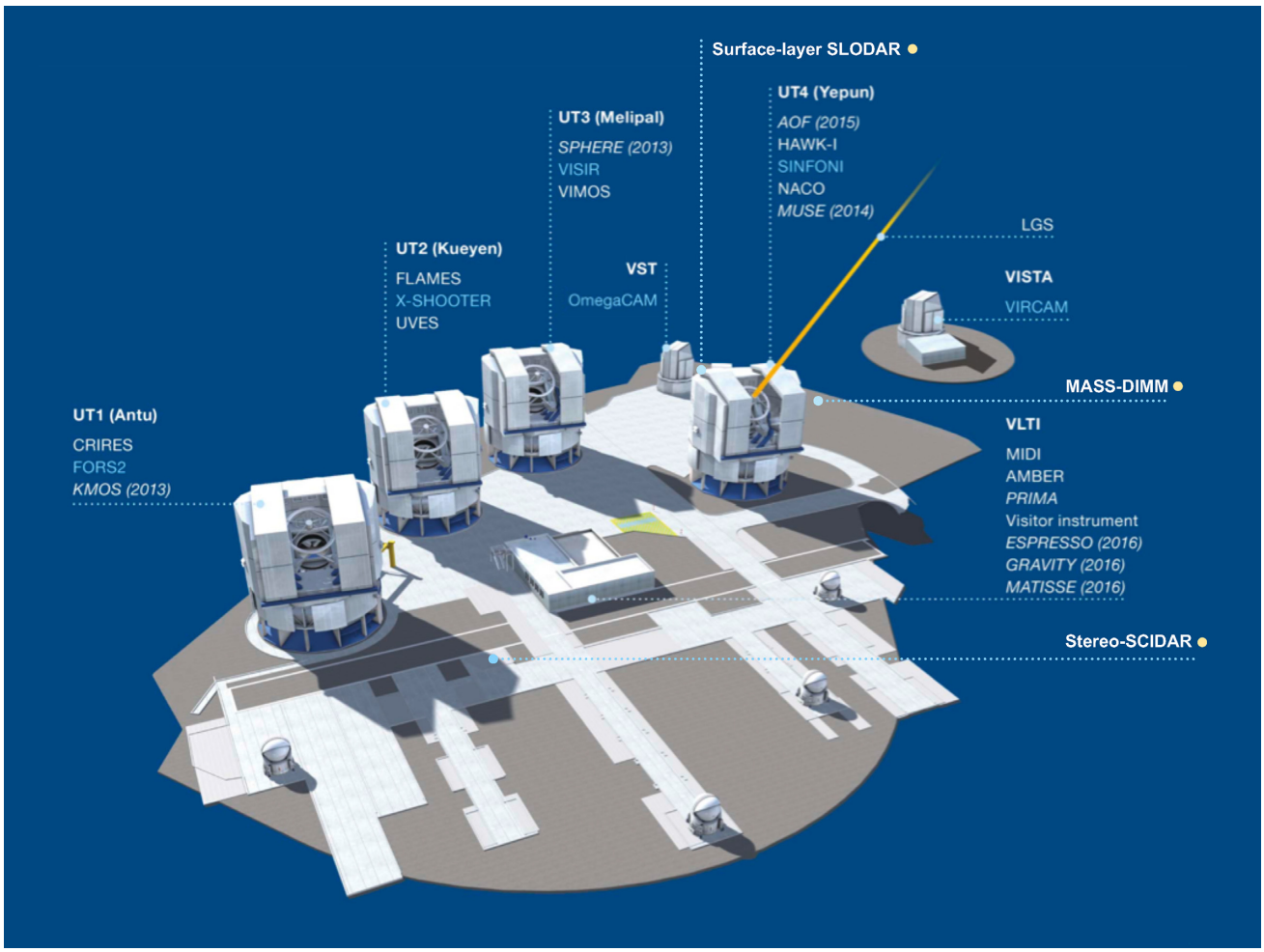

Figure 6. Overview of the instrumentation at the ESO Paranal site. Modified from original image by ESO to include the locations of the turbulence-monitoring instrumentation (indicated by yellow markers).

compare with the wind velocity measurements recovered from the Stereo-SCIDAR instrument.[1]

The ECMWF model is a non-hydrostatic model. The model is refreshed every 6 h and provides a forecast for every hour. Two-level models are produced, pressure level and model level. For the model levels, as used here, forecasts are provided at 137 altitude levels. The altitude levels are hybrid, defined as lines of constant pressure above surface pressure. The altitude resolution is generally a couple of tens of metres near the ground and a few kilometres above the tropopause.

Here, we use publicly available data from the ECMWF Re-Analysis (ERA5) catalogue. The data have 0.3 degree spatial resolution and is only available for the models produced at 06:00 and

[1] https://www.ecmwf.int/en/forecasts/data sets/

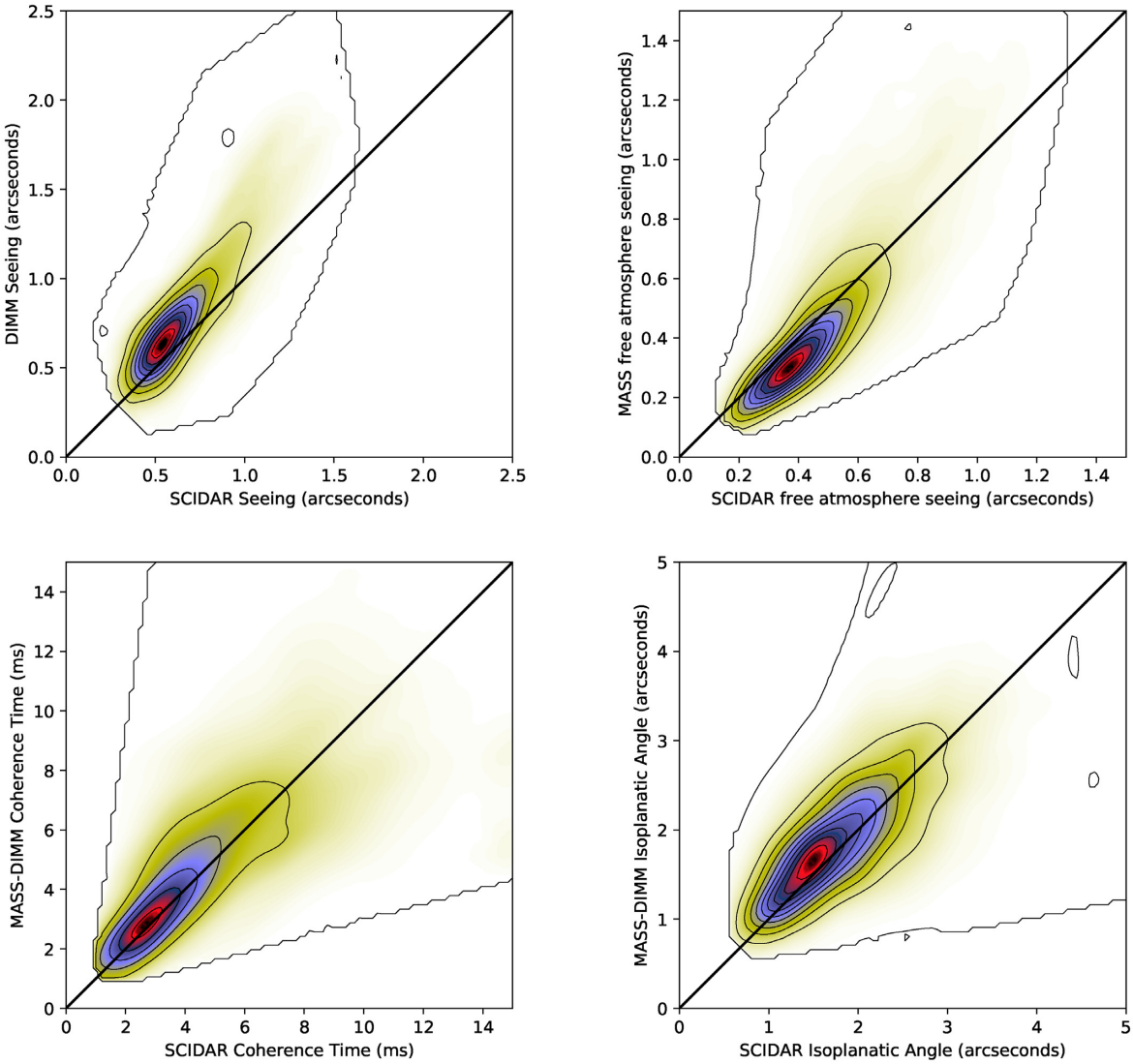

Figure 7. Astro-atmospheric parameter comparison between the MASS-DIMM and the Stereo-SCIDAR for seeing (top, left), free-atmosphere seeing (top, right), coherence time (bottom, left) and isoplanatic angle (bottom, right). The comparison metrics can be found in Table 3.

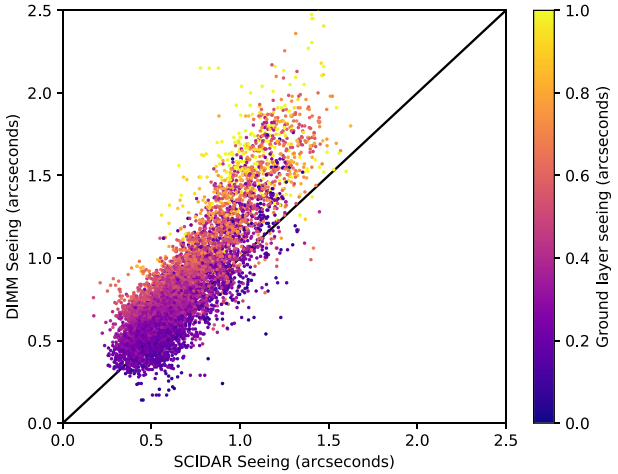

Figure 8. Comparison of the Stereo-SCIDAR and DIMM seeing, coloured by the strength of the ground layer (DIMM seeing–MASS seeing).

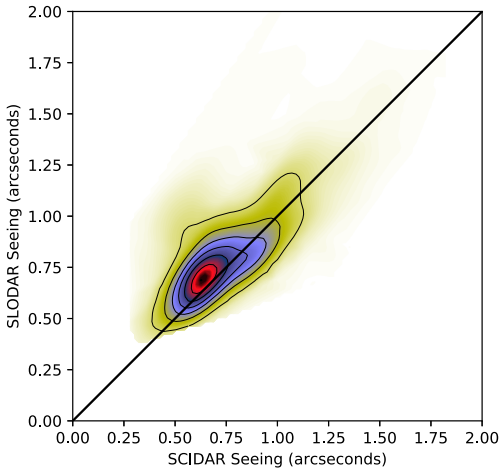

Figure 9. Comparisons of Stereo-SCIDAR and SL-SLODAR for the integrated seeing from the altitude of the AT upwards. The correlation is 0.73, bias is $-0.04''$, and RMSE is $0.2''$.

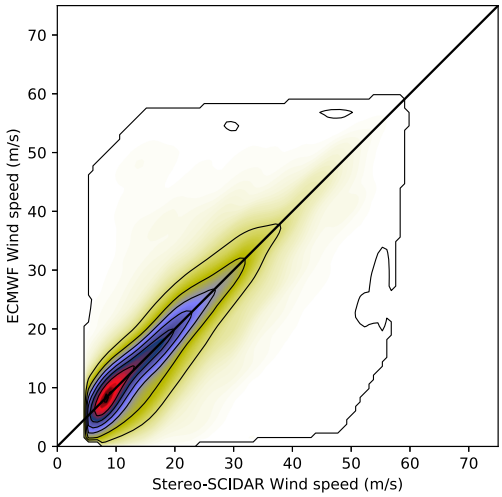

Figure 10. Comparisons of Stereo-SCIDAR recovered wind speed with the forecast wind speed from the ECMWF. The wind speed correlation = 0.82, bias = 0.41 m s^{-1}, and RMSE = 6.44 m s^{-1}.

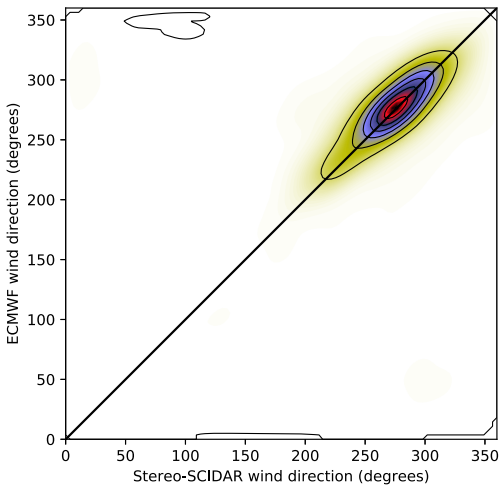

Figure 11. Comparisons of Stereo-SCIDAR recovered wind direction with the forecast wind direction from the ECMWF. The wind direction correlation = 0.77, bias = 1.59 degrees, and RMSE = 27.09 degrees.

18:00 UT, with forecasts for every hour up at 19 h. Here, we use the best case data, i.e. data that were produced at most 11 h before (for example, 06:00+11 h). To extract the parameters for the site of Cerro Paranal in the 0.3 degree grid, we linearly interpolate between the four nearest data points.

Fig. 10 shows the comparison between wind speed from the Stereo-SCIDAR and ECMWF for all altitudes, Fig. 11 shows the comparison of wind direction. The correlation values of this comparison (0.82 and 0.77 for wind speed and direction, respectively) are lower than those found for La Palma as reported in Osborn et al. (2017) (0.9 and 0.93, respectively). We also see that the RMSE of the wind direction is significantly larger at Paranal than found at La Palma. The reason for this discrepancy is due to the large wind shear within turbulent zones in the free atmosphere at Paranal, resulting in a dispersion of velocity vectors for the turbulent zone. The model does not have sufficient vertical resolution to resolve the velocity dispersion that is measured by the Stereo-SCIDAR.

5 CONCLUSIONS

In this publication, we introduce the ESO Stereo-SCIDAR and show the statistical results that describe the Paranal site. We also compare the results to several other dedicated atmospheric characterization instruments and models, namely the MASS-DIMM, Surface-Layer SLODAR, and the ECMWF wind velocity forecast. This information is of interest to existing and future instruments for the VLT at Cerro Paranal, Chile, as well as for the future AOs instrumentations for the 38 m European ELT which is being constructed approximately 20 km away.

We show high correlations between the Stereo-SCIDAR and the other instruments, with Pearson correlation coefficients between 0.60 (MASS-DIMM isoplanatic angle) and 0.84 (MASS-DIMM seeing). The median seeing, coherence time, and isoplanatic angle is found to be 0.64″, 4.18 ms, and 1.75″, respectively. We also examine the fraction of the turbulence strength in the ground layer up to various altitudes. We find that the median ground layer fraction up to 300 m, 600 m, 900 m, and 1200 m is 0.25, 0.40, 0.45, and 0.49, respectively. The ground layer fraction is critical to the performance of wide-field AOs instrumentation.

ACKNOWLEDGEMENTS

FP7/2013-2016: The research leading to these results has received funding from the European Community's Seventh Framework Programme (FP7/2013-2016) under grant agreement number 312430 (OPTICON).

Horizon 2020: This project has received funding from the European Union's Horizon 2020 research and innovation programme under grant agreement No 730890. This material reflects only the authors views and the Commission is not liable for any use that may be made of the information contained therein.

This work was supported by the Science and Technology Funding Council (UK) (ST/L00075X/1). DL acknowledges support from the UK Programme for the European ELT (ST/N002660/1). OJDF acknowledges the support of STFC (ST/N50404X/1).

We also acknowledge ECMWF for access to the weather forecast data through the MARS access system.

This research made use of python including numpy and scipy (van der Walt, Colbert & Varoquaux 2011), matplotlib (Hunter 2007) and Astropy, a community-developed core Python package for Astronomy (Robitaille et al. 2013). We also made use of the python AO utility library 'AOtools'.

REFERENCES

Avila R., Vernin J., Cuevas S., 1998, PASP, 110, 1106
Basden A., Myers R., Butterley T., 2010, Applied Optics, 49, G1
Butterley T., Wilson R. W., Sarazin M., 2006, MNRAS, 369, 835
Butterley T., Wilson R., Sarazin M ., 2015, Journal Adaptive Optics for Extremely Large Telescopes Conference Proceedings
Dali Ali W. et al., 2010, A&A, 524, A73
Derie F., Wilson R., Osborn J., Dubbeldam M., Sarazin M., Ridding R., Navarrete J., Lelouarn M., 2016, The Messenger, 166, 41
Dravins D., Lindegren L., Mezey E., Young A. T., 1997, PASP, 109, 173
European Southern Observatory 2009, Technical report, An Expanded View of the Universe
Fried D. L., 1966, J. Opt. Soc. Am., 56, 10, 1380
Gendron E., Morel C., Osborn J., Martin O., Gratadour D., Vidal F., Le Louarn M., Rousset G., 2014, in Marchetti E., Close L. M., Véran J.-P., eds, Proc. SPIE Conf. Ser., 9148, SPIE, Bellingham, p. 13
Giordano C., Vernin J., Vazquez Ramío H., Muñoz-Tuñon C., Varela A. M., Trinquet H., 2013, MNRAS, 430, 3102

Greenwood P. D., 1978, J. Opt. Soc. Am., 69, 549
Hagelin S., Masciadri E., Lascaux F., 2010, MNRAS, 407, 2230
Hunter J. D., 2007, Comput. Sci. Eng., 9, 90
Korkiakoski V., Osborn J., Grosse D., Thorn E., Piatrou P., Bennet F., Rigaut F., 2016, in van Eijk A. M. J., Davis C. C., Hammel S. M., eds, Proc.SPIE Conf. Ser., 9979. SPIE, Bellingham, p. 11
Kornilov V., Tokovinin A. A., Vozyakova O., Zaitsev A., Shatsky N., Potanin S. F., Sarazin M. S., 2003, in Wizinowich P. L., Bonaccini D., eds. Proc. SPIE Conf. Ser., 4839. SPIE. Bellingham, p. 837
Lombardi G., Sarazin M., 2016, MNRAS, 455, 2377
Lombardi G. et al., 2010, in SPIE Astronomical Telescopes and Instrumentation. p. 77334D
Maire J., Ziad A., Borgnino J., Martin F., 2007, MNRAS, 377, 1236
Masciadri E., Lascaux F., Fuensalida J. J., Lombardi G., Vázquez-Ramió H., 2011, MNRAS, 000, 1
Masciadri E., Lascaux F., Fini L., 2013, MNRAS, 436, 1968
Masciadri E., Lombardi G., Lascaux F., 2014, MNRAS, 438, 983
Masciadri E., Lascaux . F., Turchi A., Fini L., 2017, MNRAS, 466, 520
Morris T. J., 2014, in Proc. of IOP: conference series 595: Adapting to the Atmosphere
Morris T. et al., 2014, in Adaptive Optics Systems IV, 9148, SPIE, Bellingham, p. 12
Neichel B., Fusco T., Conan J.-M., 2008, J. Opt. Soc. Am., 26, 219
Osborn J., Wilson R., Butterley T., Shepherd H., Sarazin M., 2010, MNRAS, 1408, 1405
Osborn J., Butterley T., Perera S., Fohring D., Wilson R., 2015, in Adaptive Optics for Extremely Large Telescopes – Conference Proceedings, 1
Osborn J., Föhring D., Dhillon V. S., Wilson R. W., 2015b, MNRAS, 452, 1707
Osborn J., Butterley T., Townson M. J., Reeves A. P., Morris T. J., Wilson R. W., 2017, MNRAS, 464, 3998
Prieur J. L., Avila R., Daigne G., Vernin J., 2004, PASP, 116, 778
Ramió H. V. et al., 2008, ESO messenger, 132
Robitaille T. P. et al., 2013, A&A, 558, A33
Roddier F., 1981, in Progress in Optics, 19, North-Holland Publishing Co., Amsterdam, p. 281.
Sarazin M., Roddier F., 1990, A&A, 227, 294
Sarazin M., Melnick J., Navarrete J., Lombardi G., 2008, The ESO Messenger, 132, 11
Sarazin M., Cuevas O., Navarrete J., 2011, Revista Mexicana de Astronomía y Astrofísica, 41, 42
Shepherd H. W., Osborn J., Wilson R. W., Butterley T., Avila R., Dhillon V. S., Morris T. J., 2014, MNRAS, 437, 3568
Sivo G., 2014, PhD thesis, Institut de Optique
Skidmore W., Committee T. I. S. D. T. T. S. A., 2015, Res. Astron. Astrophys., 15, 1945
Tokovinin A., Kornilov V., 2007, MNRAS, 381, 1179
Tokovinin A., Bustos E., Berdja A., 2010, MNRAS, 000, 1
van der Walt S., Colbert S. C., Varoquaux G., 2011, Comput. Sci. Eng., 13, 22
Vernin J., Roddier F., 1973, J. Opt. Soc. Am., 63, 270
Vidal F., Gendron E., Rousset G., 2010, J. Opt. Soc. Am., 27, 253
Wilson R. W., 2002, MNRAS, 337, 103
Ziad A., Schö M., Chanan G. A., Troy M., Dekany R., Lane B. F., Borgnino J., Martin F. O., 2004, Appl. opt., 43, 2316

This paper has been typeset from a TEX/LATEX file prepared by the author.